Investigation of the onset of chaos in an ergodic cavity

Delft University of Technology

Bachelor final thesis

Applied Mathematics and applied physics

Freek Looman

4604350

Delft, 2021

Contents

1 Introduction **1**

2 Defining a model **2**
2.1 The physical situation . . . 2
2.2 Ray tracing . . . 3
2.3 Fourier transform . . . 3

3 Mathematical description of chaos **4**
3.1 Ergodicity . . . 4
3.2 Billiards . . . 4
3.3 Choosing coordinates . . . 5
3.4 Lyapunov Exponents . . . 6
3.5 Lyapunov exponent for quarter stadium billiards . . . 6
3.6 Lyapunov exponent for Circular billiard . . . 8

4 Behavior of a toymodel field **9**
4.1 The model . . . 9
4.2 Statistics around random waves . . . 9
4.3 Analyzing field distribution of random waves . . . 10
4.4 Analyzing field from restricted random waves . . . 11

5 Distribution of field intensity **14**
5.1 Distribution of a single pixel . . . 14
5.2 Using the Rayleigh distribution to show ergodicity . . . 16
5.3 Rayleigh distribution due to chaos . . . 19

6 Convergence of the simulation **21**
6.1 Convergence of the field . . . 21
6.2 Number of reflections needed for convergence . . . 21

7 Outlook **25**
7.1 General losses inside the cavity . . . 25
7.2 Modelling exit in quarter stadium . . . 25

8 Conclusion **28**

1 Introduction

The behavior of light is well understood and well documented in many different scenarios. Nonetheless the situations can get more complicated. We can easily calculate the electromagnetic field confined to a cubic volume by solving the wave equations. However, this is not so easy for arbitrary geometries of the boundary. The wave equation most likely does not have well defined Eigenmodes for arbitrary shape of the boundary and conditions on this boundary. This complex situation can give a chaotic field. In this bachelor thesis we are going to investigate this situation for a 2-dimensional cavity in the shape of a quarter stadium, in which light can move freely and is reflected on the boundaries. The shape of our cavity is expected to result in a really chaotic field, whose properties will be studied in detail below.

We will introduce ergodicity and compare the behaviors of a chaotic and non-chaotic cavity using ergodic properties and looking at the divergence of two neighboring trajectories. Furthermore we will look at the onset of chaos in the wave field inside the cavity and suggest a test to determine if a field is completely chaotic.

2 Defining a model

2.1 The physical situation

We are going to implement a model that explains the chaotic behavior of light in the 2D quarter stadium cavity [3] that can be seen below in figure 1. It is patterned in a silicon-on-insulator slab, as commonly used in on-chip photonics. Light in this kind of photonic system is confined to the slilicon slab in the z direction by total internal reflection at the interface between silicon and air. In the x and y direction a so-called photonic crystal confines the light. The photonic crystal can be seen as hexagonal array of holes, appearing light grey area in figure 1.
A photonic crystal is a structure of periodic dielectric materials with different refractive indices [2]. Certain wavelengths of light will destructively interfere with itself due to these periodic dielectrics. This means we will get a certain band gap in the allowed wavelengths of light that exist in the dielectric crystals. This band gap is comparable to band gaps in the energy of electrons in solids. In this experiment we will use light with a wavelength of $1550nm$ which is in the band gap of this photonic crystal.
The light enters this cavity from a feed-waveguide at the bottom left corner. In figure 1 , a second waveguide at the top-right corner can be seen, from which light can escape the cavity.
We will call the shape of this cavity the quarter stadium. This shape is chosen because this will give chaotic properties to the electromagnetic field inside of the cavity. This is because the shape of the cavity is assumed to be ergodic [5].

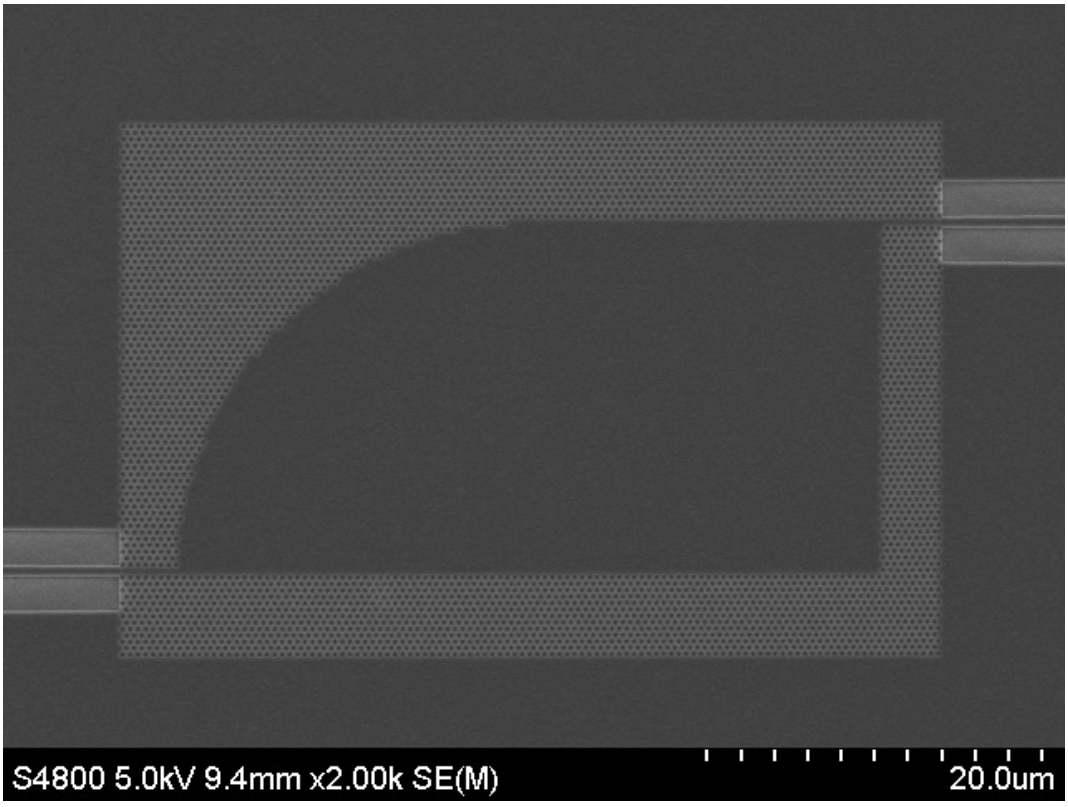

Figure 1: A scanning electron micrograph of the experimentally realized cavity which we are modelling in this thesis. The dark grey area is the silicon slab where light can travel freely and the light grey part consists of the hexagonal photonic crystal array where light reflects upon.

2.2 Ray tracing

In general the size of the system means that we are in a region where geometric optics stops to be a good approximation and wave optics is necessary to fully describe the problem. The main reason for geometric optics to stop being a good aproximation is the width of the waveguide and the wavelength of the light being on the same scale. Nonetheless, we will see that using a combination of techniques from both approaches allow us to extract a lot of information about the system.
The cavity itself can be described using geometric optics, since the cavity is $50\mu m$ long and the wavelength of the light used is $1550nm$. For this we will start with using a technique from geometric optics called ray tracing.
With ray tracing we simulate the light, as we do in geometric optics, as a ray that bounces around in our cavity. To model the effect of feeding light into the cavity trough the waveguide, which is comparable in width to the wavelength, we use a collection of rays exiting at a random angle, bounded by the diffraction limit.
For simplicity we will only calculate the electric field which is perpendicular to our cavity. The other spatial components of this field could nonetheless be calculated with Maxwell's equations. I did not focus on this aspect in this thesis.
Now to calculate this electric field we will for every bounce in our simulation add a complex plane wave with unit amplitude, which starts at position (x_0,y_0) and with a relative phase ϕ_0. The propagation direction of the wave is given by (k_x,k_y). For simplicity we will use a vector notation in the form of $\bar{x}$ for these. Now the field generated from a single wave i is given by

$$E_i(\bar{x}) = e^{j\left(\bar{k}_i \cdot (\bar{x} - \bar{x}_{0,i}) + \phi_i\right)} \tag{1}$$

where j is the imaginary number. Assuming we have n reflections, it is easy to calculate location and angles of the next ray segment by finding the intersection between boundary of the cavity and our ray. The relative phase ϕ_i between subsequent rays requires a little more work. Here we start by finding what phase the plane wave has right before interacting with the cavity boundary and add π to it. This is because the wave needs to obey a certain boundary condition known as Fresnel equations where the field is equal to 0 on the boundary. Now we can calculate the total field of a single ray that reflects n-1 times, which means we have n ray segments.

$$E(\bar{x}) = \sum_{i=1}^{n} e^{j\left(\bar{k}_i \cdot (\bar{x} - \bar{x}_{0,i}) + \phi_i\right)} \tag{2}$$

Now we are interested in the electric energy density of the field. For this we will take the absolute value of the field.

2.3 Fourier transform

To get more information from this field distribution, we will use a 2D Fourier transform.
When a wave reflects on a boundary, it changes direction. The wavelength is hereby being preserved. We know that the Fourier transform of a single plane wave is a complex-valued delta peak at a given point (k_x, k_y) in reciprocal coordinates. Because the wavelength is constant for all participating waves, this delta peak will always be on a circle with radius $|\bar{k}|$. Because of the linearity of the Fourier transform we get that the Fourier transform of the total field is zero everywhere except on the circle with radius $|\bar{k}|$.

3 Mathematical description of chaos

We already stated that the field inside the shown quarter stadium cavity is assumed to be chaotic. To discuss the ramifications of chaos we will first define what it means if something is ergodic. After this we will discuss how this relates to our quarter stadium cavity.

3.1 Ergodicity

First of all we will start with a mathematical treatment of ergodicity. This definition of ergodicity relies a lot on measure theory [5]. We will assume a map T on a probability space (X,$\mathcal{O}$,μ).
Note that a set A$\in \mathcal{O}$ is called T-invariant if $T^{-1}(A) = A$.

Definition 3.1 (Ergodicity) *A map T of probability space (X,$\mathcal{O}$,μ) is called ergodic if every T invariant set has either measure 0 or 1.*

This might seem abstract but it can be interpreted for our quarter stadium cavity. However, for this chapter we will use a billiard ball analogy. Assuming only geometric optics as first approximation of our cavity, rays travel inside the cavity the same way a billiard ball would on a billiard table with the same shape.
Let T be the map that gives the next reflection location in a trajectory and let A be a trajectory. For now we briefly assume that A is T invariant, we will show this in the next chapter. Now if T, or in other words the stadium, is ergodic, then all these possible trajectories have measure 0 or 1. If the trajectory has measure 0 it reflects at finitely many distinct locations and is periodic. If it has measure one it bounces almost everywhere on the boundary and becomes chaotic.

Ergodicity also has an important property, for which the mathematical description does not give more insight in this thesis. However we will use this philosophy in the next chapter.

Theorem 3.1 (Birkhoff Ergodic Theorem) *The time average will converge to the space average of ergodic processes.*

This theorem is powerful. By assuming ergodicity we can try to find a time average of a property in our simulation on a single point and assume that it converges to the space average of this same property.

3.2 Billiards

Before we can use anything ergodicity related, we will first properly define our billiard ball trajectory. We start by defining our billiard table $Q \subset \mathbf{R}^2$ which we assume is an open, bounded and connected set. This billiard table has a boundary $\Gamma = \delta Q$ which is made of a collection of disjoint smooth compact curves. The end points of these smooth compact curves can be non-smooth points such as corners in a billiard. The set of all these points we call Γ^*.
We will need to define a trajectory of our so-called billiard ball on our table. At a given time the ball is at location $q \in Q$ and has a velocity $v \in \mathbf{R}^2$. However since we are only interested in the trajectory and not the time it takes we will assume that v is on a unit circle. We call S^1 the set containing these v.
We only need to define what happens when a ball bounces. This bounce will follow normal dynamics where angle of incidence is also the outgoing angle. Now we can talk about phase space $\mathcal{M} = \bar{\delta Q} \times S^1$, which contains every combination of velocity and location on our billiard table. We can now construct a single trajectory, or flow, Φ^t in this phase space. Note that in Φ^t t can be seen as time.
This flow can also be defined by the locations and angles of the reflections. For this we construct a second phase space describing the same flow but only defined at the boundary of the billiard table.

$$M = \{x = (q, v) \in \mathcal{M} : q \in \delta Q \text{ and } \langle v, n(q) \rangle \geq 0\} \tag{3}$$

Here, $n(q)$ is the inward orientated normal vector and $\langle \cdot, \cdot \rangle$ is the inner product. This makes sure a bounce is going in the right direction.
We will define a map from one reflection to the next reflection in a single flow. Let $T : M \to M$ be a map such that for $x \in M$ we get $Tx = \Phi^{\tau(x)}x$ where $\tau(x)$ is the time for which the flow is on the next bounce defined by the following formula:

$$\tau(x) = \{t > 0 : \Phi^t x \in M\} \tag{4}$$

Note that also the angle after every reflection changes. These reflections will obey that the angle of incidence is the same as the outgoing angle.
Looking at trajectories instead of single reflections, we let A be a trajectory defined as follows:

$$A = \{..., T^{-2}(x_0), T^{-1}(x_0), x_0, T(x_0), T^2(x_0), T^2(x_0), ...\} \tag{5}$$

Note that we can now conclude that every trajectory is T-invariant because $T^{-1}(A) = A$.

This map T is completely defined by the shape of the stadium, so this means that a stadium can be in one of two categories. A stadium is ergodic or it is non-ergodic. A Bunimovich stadium is an example of an ergodic cavity and a circle is known to be non-ergodic [[5]]. The Bunimovich stadium is build from two half circles connected by two straight lines as can be seen in figure [2]

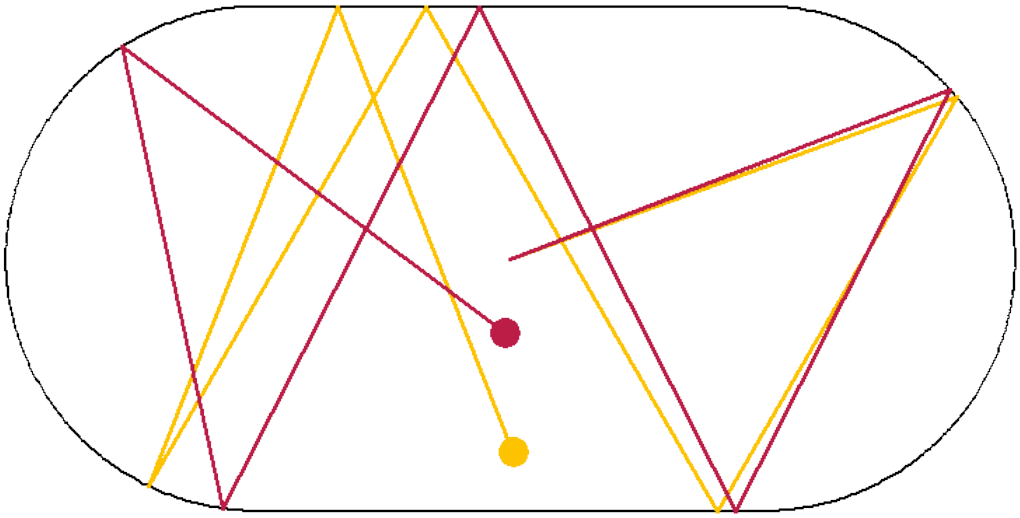

Figure 2: A Bunimovich stadium with 2 starting rays (red and yellow) with slightly different initial direction. Image adapted from https://blogs.ams.org/visualinsight/2016/11/15/bunimovich-stadium/

Now we can finally say something about an ergodic billiard. We have seen that every trajectory is T-invariant when T is a reflection map and we will assume it is ergodic. Now every trajectory has measure 0 or measure 1. This means that almost every trajectory is dense in phase space, and chaotic.

3.3 Choosing coordinates

Up to now we have defined our phase space using the location of reflection q and velocity v. We will redefine our angle by defining it by the angle between the outgoing travel direction and the normal from where it reflects which we call θ. Every possible point in phase space M can be described using

this θ, so we will redefine M:

$$M = \left\{ x = (q, \theta) \in \mathcal{M} : q \in \delta Q \; and \; -\frac{\pi}{2} < \theta < \frac{\pi}{2} \right\} \tag{6}$$

3.4 Lyapunov Exponents

We will try to show that our stadium is chaotic using Lyapunov exponents [[1]]. Lyapunov exponent λ is a way to estimate if two nearby trajectories in phase space will converge or diverge over time. This estimate is given by

$$||\delta Z(t)|| = e^{\lambda t}||Z(0)|| \tag{7}$$

where $\delta Z(t)$ is the difference in 2 neighboring trajectories. We can conclude that we will get converging flows when $\lambda < 0$. This thesis is focused on chaos so we will be looking for $\lambda > 0$ because we want trajectories to diverge.

Note that the Lyapunov exponent is a property of a single flow in phase space and not the phase space itself. We can speak of a chaotic field when all flows in phase space diverge, or in other words have a positive Lyapunov exponent. An example of a trajectory with positive Lyapunov exponent can be seen in figure 2.

We so far studied the system using a discrete time map. To evaluate the Lyapunov exponent of a given flow, we start with assuming δZ_0 and want to find δZ_1. If we have this we can repeat the process n times to get δZ_n. For discrete time steps this is the Jacobian of the map, which will be a 2 by 2 matrix, for our billiards given by

$$J^n(Z_0) = J(Z_{n-1})J(Z_{n-2}) \cdots J(Z_2)J(Z_1) \tag{8}$$

From this matrix we will try to approximate the Lyapunov exponent. For this we will use our largest in absolute value eigenvalue Λ_1 of this total Jacobian. Rewriting equation (7) will give us the following

$$\lambda(Z_0) \simeq \frac{1}{n} ln\, |\Lambda_1(Z_0, n)| \tag{9}$$

3.5 Lyapunov exponent for quarter stadium billiards

To find the Lyapunov exponent for trajectories in the quarter stadium billiard we only need to define the Jacobian matrix $J(Z_i)$ and the distance between two directories δZ_i for some i. We will define δZ_i by the difference in traveling angle θ and distance between the two close-by trajectories z_i.

$$\delta Z = \begin{pmatrix} \delta z \\ \delta \theta \end{pmatrix} = \begin{pmatrix} z - z' \\ \theta - \theta' \end{pmatrix} \tag{10}$$

Now we will need to find the Jacobion matrix. We will define this by defining a Jacobian for the trajectory traveling freely inside of the cavity and a Jacobian describing a reflection.
First we will look at this Jacobian matrix for a free traveling path $M_T(x_n)$ just until the next reflection. The angle of two close rays does not change during free travel. However they will separate depending on the angle difference

$$\frac{d\delta\theta}{dt} = 0, \quad \frac{d\delta z}{dt} = \delta\theta \tag{11}$$

Integrating this over time between two reflections we get the following:

$$\delta\theta_n = \delta\theta_{n-1}, \quad \delta z_n = \delta z_{n-1} + \tau\delta\theta_{n-1} \tag{12}$$

where τ is the time traveled. This is equivalent to the distance traveled because we chose the speed to be 1. Now we will rewrite this in matrix notation

$$M_T(x_n) = \begin{bmatrix} 1 & \tau \\ 0 & 1 \end{bmatrix} \tag{13}$$

Now we need to find the Jacobian matrix from reflection. Note that due to reflection the distance between the two rays stays the same, however they switch position so δz gets a minus sign. This is also the case for $\delta\theta$. Interesting is the change in $\delta\theta$.

$\delta\theta$ changes depending on the difference in angle of the normal of the cavity wall called $\delta\phi$, given by $\delta\theta = 2\delta\phi$. For finding $\delta\phi$ i refer the reader to chapter 9 of the chaos book [[1]], which results in $\delta\phi_n = \frac{\delta z_n}{\rho_n cos(\phi_n)}$. Note that ρ_n is defined as the radius of the circle defining the local curvature. In this thesis we will only look at reflection on the inside of a circle, making ρ non-positive. Combining all of this we will get the Jacobian matrix

$$M_R(x_n) = -\begin{bmatrix} 1 & 0 \\ r_n & 1 \end{bmatrix} \tag{14}$$

where $r_n = \frac{2}{\rho_n cos(\phi_n)}$. Now we can find the total Jacobian matrix for one reflection to be $M(x_n) = M_T(x_n)M_R(x_n)$. Using equation (8) we get the total Jacobian for a trajectory by traveling freely and reflecting p times from starting point x_0

$$M_p(x_0) = (-1)^p \prod_{n=p}^{1} \begin{bmatrix} 1 & \tau_n \\ 0 & 1 \end{bmatrix} \begin{bmatrix} 1 & 0 \\ r_n & 1 \end{bmatrix} \tag{15}$$

We can now calculate our estimated Lyapunov exponent for trajectories in our quarter stadium using equation (9). We will do this for 100 random starting points and look at the evolution of this Lyapunov exponent over 1500 reflections. The results can be seen in figure 3. The Lyapunov exponent of these simulations seem to converge between 0.02 and 0.05. All of these are clearly positive. From this result we assume the exponent to be positive almost everywhere. This means that the quarter stadium is chaotic.

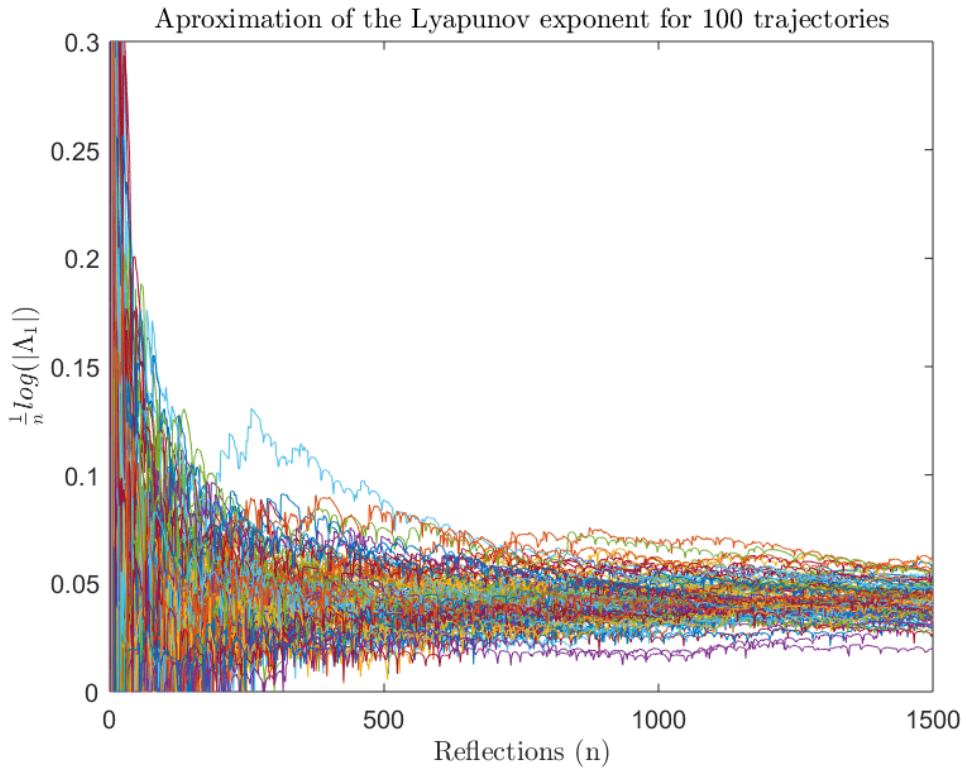

Figure 3: The Lyapunov exponent approximated for trajectories in the quarter stadium. 100 trajectories are simulated for 1500 reflections and shown as different colors in the plot. The Lyapunov exponent seems to converge between 0.02 and 0.05 which implies a chaotic behavior.

3.6 Lyapunov exponent for Circular billiard

We have shown a positive Lyapunov exponent for the quarter stadium. Now we will look at the Lyapunov exponent for the circular stadium, which is known to be non-ergodic as stated before. A trajectory in a circular stadium is rather simple. Every reflection preservers the angle of reflection ϕ, the curvature ρ and the travel distance τ. We will simplify equation 15 using this knowledge to get the Jacobian matrix for p reflections inside a circular stadium

$$M_p(x_0) = (M_1(x_0))^p = \left(- \begin{bmatrix} 1 & \tau \\ 0 & 1 \end{bmatrix} \begin{bmatrix} 1 & 0 \\ r & 1 \end{bmatrix} \right)^p \tag{16}$$

We can simplify this further by calculating τ and r. Using some simple geometry we get $\tau = 2R\cos\phi$ and $r = \frac{2}{-R\cos\phi}$ where R is the radius of our circular stadium. Inserting this in equation 16 leads to

$$M_1(x_0) = - \begin{bmatrix} 1 & 2R\cos\phi \\ 0 & 1 \end{bmatrix} \begin{bmatrix} 1 & 0 \\ \frac{2}{-R\cos\phi} & 1 \end{bmatrix} = - \begin{bmatrix} -3 & 2R\cos\phi \\ \frac{-2}{R\cos\phi} & 1 \end{bmatrix} \tag{17}$$

Using elementary linear algebra we can find that the Eigenvalue of $M_p(x_0)$. This results in

$$Eig\left(M_p(x_0)\right) = \left(Eig\left(M_1(x_0)\right)\right)^p \tag{18}$$

Calculating the eigenvalue of $M_1(x_0)$ using equation 17 we get that $Eig(M_1(x_0)) = \{1\}$. We conclude using equation 16 that $Eig(M_p(x_0)) = \{1\}$ for all p. This means that we get a maximum Lyapunov exponent using equation 9 of 0. This means that nearby trajectories are not diverging. They can be converging or keep the same distance. This is as expected for a non-ergodic billiard.

4 Behavior of a toymodel field

4.1 The model

With the additional knowledge from the previous chapter about chaos and ergodicity we will look at a simplified toy model for our chaotic cavity. We will use this model to get more experience with the behavior of chaotic fields.

The model we described in chapter 2 has two parts. In the first part we calculate a trajectory, and in the second part we will add a complex plane wave for every reflection. In this toy model we will look at this second part. This will be done by assuming random waves which are independent of each other. For this we will simplify formula (1) using $\phi'_j = \phi_j - k_j \cdot x_{0,j}$ to get the following

$$E_j(\bar{x}) = e^{i\left(\bar{k}_j \cdot (\bar{x} - \bar{x}_{0,j}) + \phi_i\right)} = e^{i\left(\bar{k}_j \cdot \bar{x} + \phi'_j\right)} \tag{19}$$

If we assume our reflection location and phase ϕ to be random and independent we can also assume that ϕ' can be seen as a single random variable. This means we can create a random wave using only 2 parameters. These are the angle the plane wave is traveling, determining $\bar{k_j}$, and the phase ϕ'. Note that if we take a Fourier transform of a single wave, we will also get the phase ϕ'.

For every single ray we will use in this simulation, a single complex wave is added with randomly distributed angle ($\bar{k_j}$) and phase (ϕ').

Now that the basics of this model are clear we will look at mathematical approximations that allow us to gain further insight into the dynamics of the system.

4.2 Statistics around random waves

We will start by assuming a random field. This means that for every wave the angle ($\bar{k_j}$) and phase (ϕ') are uniformly and independently distributed.

We will now say something about the field at a single fixed location inside our simulation. To calculate the field on this single location we will add up all the values of every generated plane wave on this location. Since we have random waves, we can conclude that every wave adds up a value from the complex unit circle. Note that we still assume every single wave to be independent. Let stochastic variable X_j be the value of the random wave j on a fixed location. We reasoned that X_j is a random number on the unit circle for each j. We will formally define this using a stochastic variable ϕ_i which is uniformly distributed between 0 and 2π

$$X_j = e^{i\phi_j} \tag{20}$$

The intensity of the field at this location is then given by

$$Z = \left| \sum_{i=1}^{n} X_i \right| \tag{21}$$

We want to know the expected value, and variance of Z. We will use the notation $E(Z)$ and $Var(Z)$ for these, respectively. We start with finding the expected value of Z^2

$$E(Z^2) = E\left(\left| \sum_{i=1}^{n} X_i \right|^2 \right) = E\left(\sum_{i=1}^{n} X_i \cdot \sum_{j=1}^{n} \bar{X_j} \right) = E\left(\sum_{i=1}^{n} |X_i|^2 + \sum_{i \neq j}^{n} X_i \bar{X_j} \right) \tag{22}$$

Now we utilize the independence of X_i and X_j

$$E\left(\sum_{i=1}^{n}|X_i|^2+\sum_{i\neq j}^{n}X_i\bar{X}_j\right)=\sum_{i=1}^{n}E\left(|X_i|^2\right)+\sum_{i\neq j}^{n}E\left(X_i\bar{X}_j\right)=n+\sum_{i\neq j}^{n}E(X_i)E(\bar{X}_j)=n \tag{23}$$

To get the expected value of Z we will use Jensens inequality [6] to see:

$$E(|Z|)\leq\sqrt{E\left(|Z|^2\right)}=\sqrt{n} \tag{24}$$

Also, for the variance:

$$Var(|Z|)=E(|Z|^2)-E(|Z|)^2 \tag{25}$$

Noting that $0\leq E(|Z|)\leq\sqrt{n}$ we get:

$$0\leq Var(|Z|)\leq n \tag{26}$$

From this result we can see that the standard deviation and the expected value of $|Z|$ is at most $\sqrt{n}$ dependent for large enough n.
There is also reason to suspect that both need to be $\sqrt{n}$. The reason for this starts by assuming that $E(Z)$ has a smaller dependency. This will mean $Var(Z)$ needs to eventually be $\sqrt{n}$ dependent.
We will show this by assuming $E(|Z|)=a\cdot n^b$ where $b<\frac{1}{2}$. now for large enough n we get using equation (25) the following.

$$std(|Z|)=\sqrt{n-a\cdot n^{2b}}\approx\sqrt{n} \tag{27}$$

This argument goes both ways. So this means that at least one of the two is $\sqrt{n}$ dependent.

4.3 Analyzing field distribution of random waves

We will now use the model described in the beginning of this chapter to analyze the field using a uniform distribution in angle and phase. One such generated field can be seen in figure 4. We will also test wether our estimation in equation 24 and equation 26 hold when we look at the collection of 100 by 100 pixels from one simulated field.

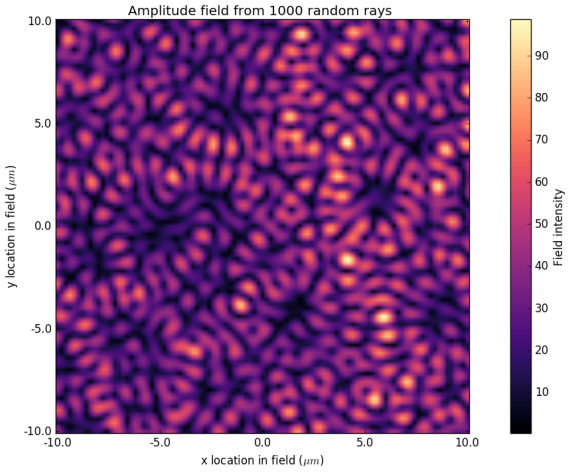

Figure 4: A simulation of a field calculated from the interference of 1000 waves with random angle and phase. The amplitude of the field highlights the constructive and destructive interference of the waves at different points in space, resulting in a chaotic pattern.

Evaluating the field and extracting the average and standard deviation of the field for different number of waves, n, results in the expected values. Both the average and standard deviation have the n dependency expected from the calculation of the single pixel. This behavior can be seen in figure 5.

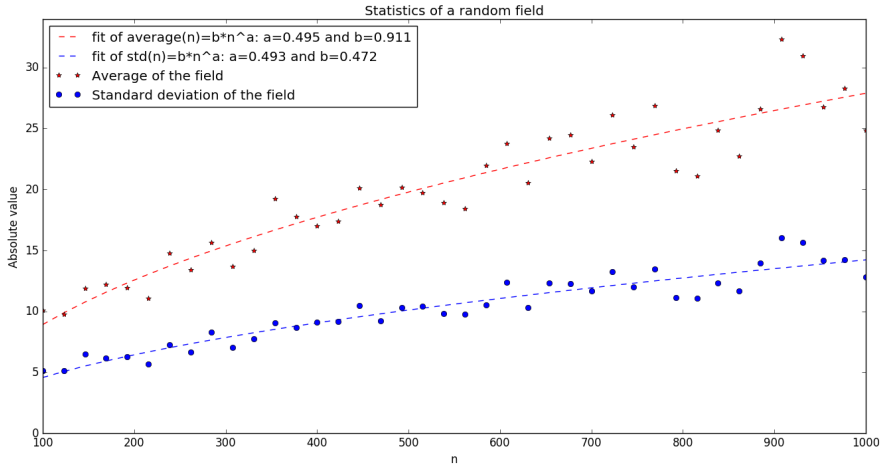

Figure 5: The number of waves n against the the average and standard deviation of the absolute value of the field. The n dependency follows the results we found in the earlier analysis.

Note that this $\sqrt{n}$ follows equations (24) and (26). Both the expected value and the standard deviation seem to depend on the $\sqrt{n}$.

4.4 Analyzing field from restricted random waves

In the previous subsection we only analyzed the field for waves with properties from a uniform distribution. However, we can also investigate if changing this distribution matters for the chotic nature of the field. We implement this by excluding certain values for the angles of the waves or certain phases. First we will exclude waves from certain angular ranges. In this case we will exclude waves with direction of travel θ between 0 and $\frac{\pi}{2}$. This gives a angle dependency of the field which can be seen in figure 6.

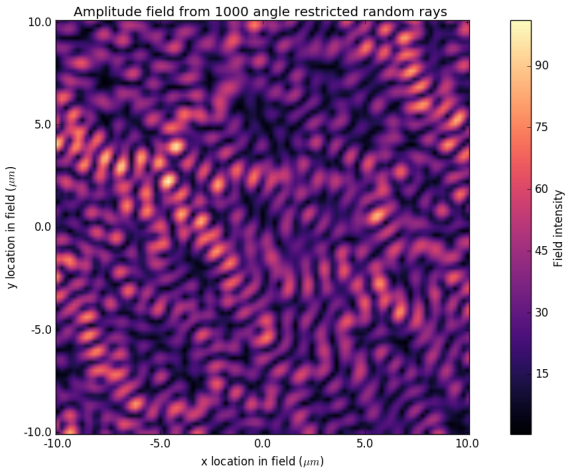

Figure 6: A simulation of a field calculated from 1000 waves with random phase. The angle of the waves is random but no waves have angle between 0 and $\frac{\pi}{2}$ with respect to the x axis.

The n dependency of this restricted field can be seen in figure 7. This is not notably different from figure 5. This means that this kind of gap in angle space does not influence our statistics and is not of interest.

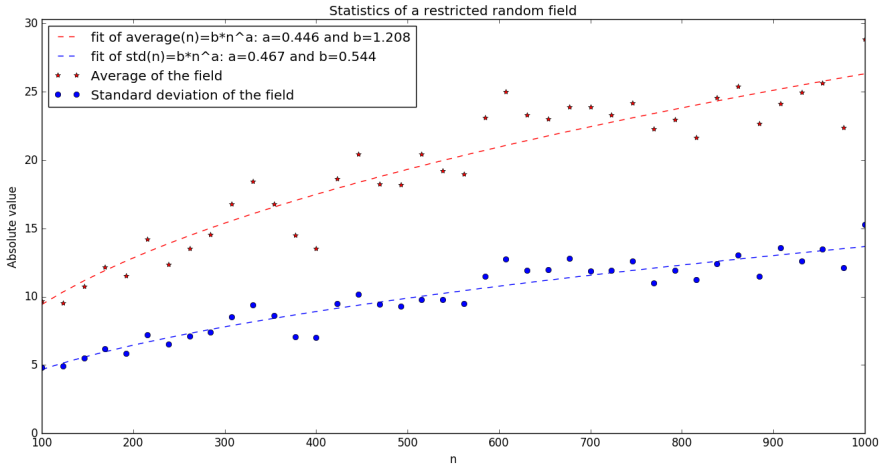

Figure 7: The n dependency of the standard deviation and expected value of an angle restricted field. Angles between 0 to $\frac{\pi}{2}$ with the x axis are removed.

We will also perform this evaluation while excluding certain phases. The phases ϕ between 0 and $\frac{\pi}{5}$ are excluded. This gives a far more interesting result which can be seen below.

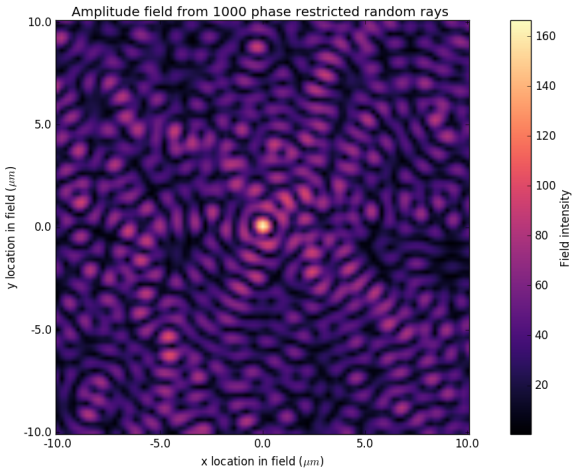

Figure 8: A simulation of a field calculated from 1000 waves with random angle. The phase is now restricted such that no phase between 0 and $\frac{\pi}{5}$ are present. Due to these restrictions the intensity peak will always be in the origin.

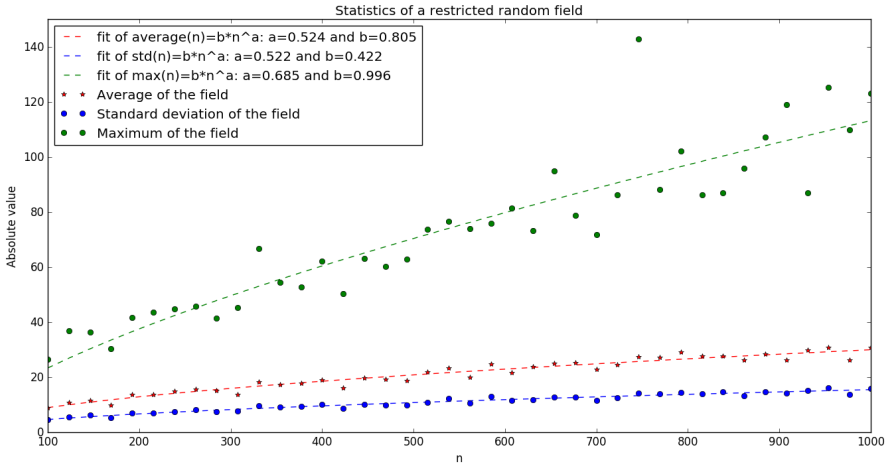

Figure 9: The number of waves n against the the average, standard deviation and maximum of the absolute value of the field. The n dependency is slightly larger compared to the situation with no restriction. The n dependency of the maximum in the simulations stated before is approximately $\sqrt{n}$ just like the average and standard deviation. This simulation has a n dependency of the maximum of the field of 0.685.

This strongly resembles a rogue wave [3]. A rogue wave is a high peak in field intensity, several times above the average of the field. This means that to find a rogue wave we could also look for a gap in phase space from our simulations. Also interesting is that the maximum of the field depends on a larger factor of n, meaning that the peak will have a relative higher amplitude for a larger number of waves. However, The peak in intensity is always on the same spot with these restrictions. This might be resolved by making the phase and angle dependent variables.

5 Distribution of field intensity

5.1 Distribution of a single pixel

In the previous chapter we looked at the average and standard deviation of random fields. It would be more insightful if we could make statements about the intensity distribution of a field. For this we will derive an intensity distribution for a random pixel inside of the cavity.
It is known that the Rayleigh distribution is common when talking about random waves [3]. The density function for this distribution is as shown in equation 28. The general Rayleigh distribution we are talking about has the following probability density:

$$f(x,\sigma) = \frac{x}{\sigma^2} e^{\frac{-x^2}{2\sigma^2}}, x \geq 0 \tag{28}$$

This distribution has a mean of $\sigma\frac{\pi}{2}$ and a variance of $\sigma^2\frac{4-\pi}{2}$. σ is the free parameter in this distribution, which controls the width.

We start this estimation by using theorem 3.1, the Birkhoff ergodic theorem. We will assume ergodicity such that the time average converges to the space average. For the time average we will calculate what intensity distribution we expect on a given pixel. We will compare this to the intensity distribution of a single run, the space average in this case.

We now want to know the distribution of the the intensity on a given pixel Z. To evaluate this we will need a few additional theorems.

Theorem 5.1 (Multivariate central limit theorem) *Let Y_i for $i = 1, 2, ..., n$ be a collection of independent random vectors of dimension k. These vectors have expectation μ, a finite covariance matrix Σ and an average $\bar{Y}_n$. The central limit theorem for vectors states*

$$\sqrt{n}(\bar{Y}_n - \mu) \xrightarrow{d} N_k(0, \Sigma)$$

where $\xrightarrow{d}$ means converges in distribution and $N_k(0,\Sigma)$ is the k-dimensional normal distribution.

Theorem 5.2 *If X is a continuous random variable with density function f_X and g is a strictly increasing and differentiable function from $\mathbb{R}$ to $\mathbb{R}$, then Y=g(X) has density function*

$$f_Y(y) = f_X\left(g^{-1}(y)\right)\frac{d}{dy}[g^{-1}(y)]$$

We will use the following theorem which is not defined in most common probability books. However it is really useful and easily understandable. This theorem has been proven in chapter 4 of Statistical tools [4].

Theorem 5.3 (Continuous mapping theorem) *Let g be a continuous function and let Y_n and Y be stochastic variables. Then*

$$Y_n \xrightarrow{d} Y \implies g(Y_n) \xrightarrow{d} g(Y)$$

For this proof we will introduce a notation where we see the complex variables as a real valued vector $Z = (R, I)$, where R is the real part and I the complex part of Z. Therefore let there be for every reflection a $X_i = (R_i, I_i)$ where this is the contribution of a single ray i to the field on the given pixel.

Note that X_i is defined differently than in equation (20). However, R_i and I_i will be defined in a similar way using ϕ_i.

$$R_i = \cos\phi_i \tag{29}$$

$$I_i = \sin\phi_i \tag{30}$$

$$Z = \left\| \sum_{i=1}^{n} X_i \right\| \tag{31}$$

Additionally, we use the following notation

$$\bar{R} = \frac{1}{n}\sum_{i=1}^{n} R_i \tag{32}$$

$$\bar{I} = \frac{1}{n}\sum_{i=1}^{n} I_i \tag{33}$$

We start by determining the covariance matrix Σ of the stochastic vector X_i.

$$\Sigma = \begin{pmatrix} Var(R_i) & Cov(R_i, I_i) \\ Cov(I_i, R_i) & Var(I_i) \end{pmatrix} \tag{34}$$

We can then use these expected value calculations as an intermediate step.

$$E(R_i) = \int_0^{2\pi} \cos(\phi_i)\frac{1}{2\pi}d\phi_i = 0 \tag{35}$$

$$E(I_i) = \int_0^{2\pi} \sin(\phi_i)\frac{1}{2\pi}d\phi_i = 0 \tag{36}$$

$$E(R_i I_i) = \int_0^{2\pi} \cos(\phi_i)\sin(\phi_i)\frac{1}{2\pi}d\phi_i = 0 \tag{37}$$

Now to conclude the variance and covariance

$$Var(R_i) = E(R_i^2) - E(R_i)^2 = \int_0^{2\pi} \cos^2(\phi_i)\frac{1}{2\pi}d\phi_i = \frac{1}{2} \tag{38}$$

$$Cov(R_i, I_i) = E(R_i I_i) - E(R_i)E(I_i) = 0 \tag{39}$$

Since the covariance is symmetric and the calculations for $Var(I_i)$ is almost identical to those for $Var(R_i)$ and gives the same result. Now we know that the covariance matrix is finite. This means we can and will use the central limit theorem to conclude the following:

$$\sqrt{2n}(\bar{R}, \bar{I}) \xrightarrow{d} N_2(0, \mathbf{I}_2) \tag{40}$$

where $\mathbf{I}_2$ is the identity matrix of size 2. By utilizing the continuous mapping theorem [5.3] using $g(x, y) = x^2 + y^2$ on $(\sqrt{2n}\bar{R}, \sqrt{2n}\bar{I}) = \sqrt{2n}(\bar{R}, \bar{I})$ we get the following

$$(\sqrt{2n}\bar{R})^2 + (\sqrt{2n}\bar{I})^2 \xrightarrow{d} \chi_2^2 \tag{41}$$

Note that for the computation of $g(N_2(0, \mathbf{I}_2))$ we use that $N_2(0, \mathbf{I}_2) = (U, V)$, where U and V are independent and standard normally distributed, which implies $g(N_2(0, \mathbf{I}_2)) = U^2 + V^2 = \chi_2^2$ where χ_2^2

is the Chi-squared distribution of degree 2.
We will rewrite

$$(\sqrt{2n}\bar{R})^2+(\sqrt{2n}\bar{I})^2=\left(\sqrt{\frac{2}{n}}n\bar{R}\right)^2+\left(\sqrt{\frac{2}{n}}n\bar{I}\right)^2=\frac{2}{n}\left(\sum_{i=1}^{n}R_i\right)^2+\frac{2}{n}\left(\sum_{i=1}^{n}I_i\right)^2=\frac{2}{n}\left\|\sum_{i=1}^{n}X_i\right\|=\frac{2}{n}Z^2 \tag{42}$$

This means that $\frac{2}{n}Z^2 \xrightarrow{d} \chi_2^2$. If we subsequently use the continuous mapping theorem again with $g(x)=\sqrt{x}$ and the knowledge that the root of a χ_2^2 distribution is a χ_2 distribution, which is a standard Rayleigh distribution. We get that $\sqrt{\frac{2}{n}}Z$ is standard Rayleigh distributed.

Now we will use theorem [5.2] in combination with the continuous mapping theorem to distribution Y where Z converges towards. Let X be standard Rayleigh distributed we will use $g(x)=\sqrt{\frac{n}{2}}x$, leading to

$$f_Y(y)=\frac{2y}{n}e^{\frac{-y^2}{n}}=\frac{y}{\left(\sqrt{\frac{n}{2}}\right)^2}e^{\frac{-y^2}{2\left(\sqrt{\frac{n}{2}}\right)^2}} \tag{43}$$

This means Z converges in distribution to a Rayleigh distribution with parameter $\sigma=\sqrt{\frac{n}{2}}$. Thus,

$$E(Z)=\frac{\pi\sqrt{n}}{2\sqrt{2}}\approx 1.11\sqrt{n} \tag{44}$$

$$Var(Z)=\frac{(4-\pi)n}{4}\approx\left(0.46\sqrt{n}\right)^2 \tag{45}$$

This result can also be seen from our simulation for which the results are indicated in figure 5, and are in good agreement with the theoretically predicted values. This means the calculated statistics of a random field and our simulation from this same field align well and is a direct hint towards this field being ergodic. This is in this case trivial, because we simulated completely random waves which are per definition ergodic.

5.2 Using the Rayleigh distribution to show ergodicity

First of all we will look at fully random waves. We will fit a Rayleigh distribution to the intensity distribution of a simulation and compare this to our theoretical distribution on a single pixel for the same amount of reflections. This can be seen in figure 10.

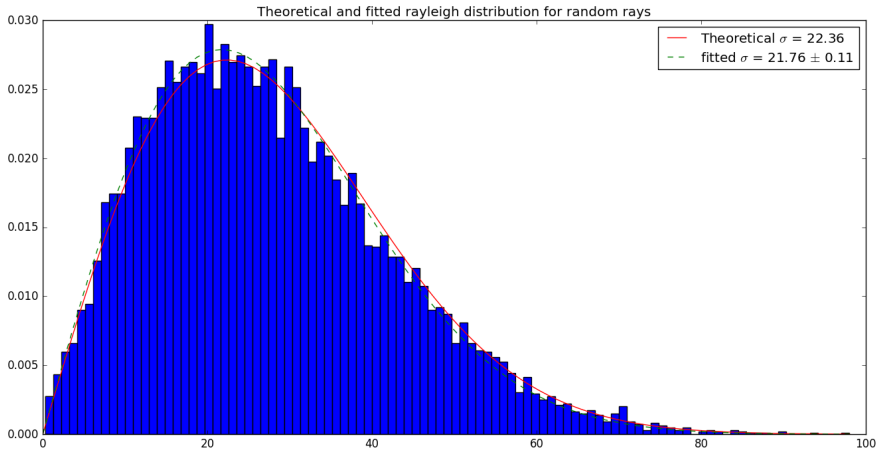

Figure 10: Histogram of the intensity of 100 by 100 pixels from a simulation with 1000 random rays. The simulation seems to follow the theoretical Rayleigh distribution.

The simulation gives the expected result, with the same distribution as the theoretical distribution calculated for a single pixel.

We have shown that our simulated random field seems to be ergodic. We conclude from this that ergodic fields show us the predicted Rayleigh distribution for the intensity. However, this conclusion does not allow us to claim that every field with Rayleigh distribution is ergodic. We therefore will look in a next step at non-chaotic and non-ergodic fields.
For this we will investigate a circle stadium, which is non-ergodic as earlier stated. Due to its symmetries it does not fill phase space. This stadium gives the field shown in figure 11.

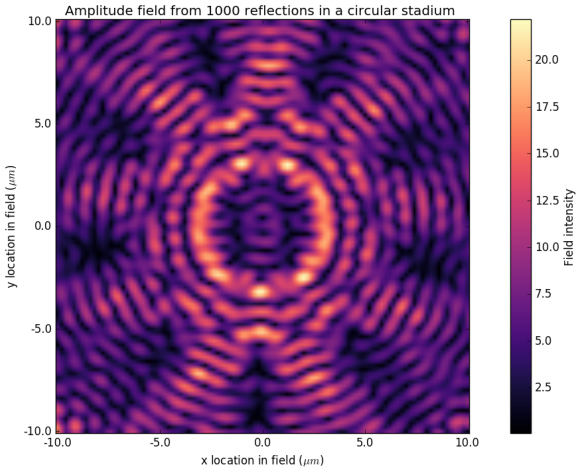

Figure 11: A simulation of a field calculated from 1000 reflections in a circular stadium. The field approaches the expected axial symmetry.

After simulating 1000 reflections the field approaches axial symmetry which is expected in this

stadium geometry. We will now look at the intensity distribution and compare this to the previously calculated number of waves. We will additionally fit a Rayleigh distribution to this data and see how this compares to the theoretically calculated distribution.

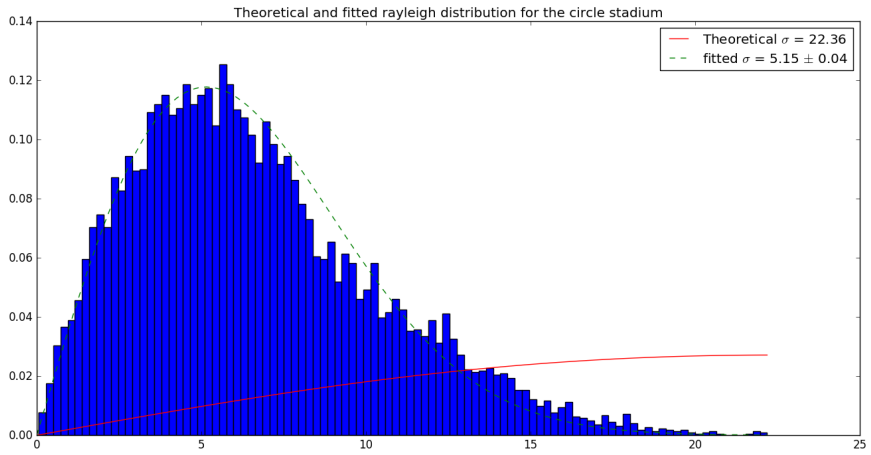

Figure 12: Histogram of the intensity of the pixels from a simulation in a circle stadium with 1000 reflections. This histogram follows a Rayleigh distributed but with a much lower σ than expected for a fully random field.

While the distribution can be approximated by a Rayleigh distribution, it does not follow the theoretically expected distribution due to a difference in its parameter σ.

This means that following a Rayleigh distribution is not a strong enough criteria for a field to be ergodic, but is rather connected to the general behavior of the field. However, the sigma parameter of the distribution seems to be a measure of ergodicity, with a smaller parameter corresponding to an overall lower mean intensity. This is linked to the dominating constructive and destructive interference in field distributions with high symmetry.

Conducting this test for the quarter stadium instead results in the data which can be seen in figure 13.

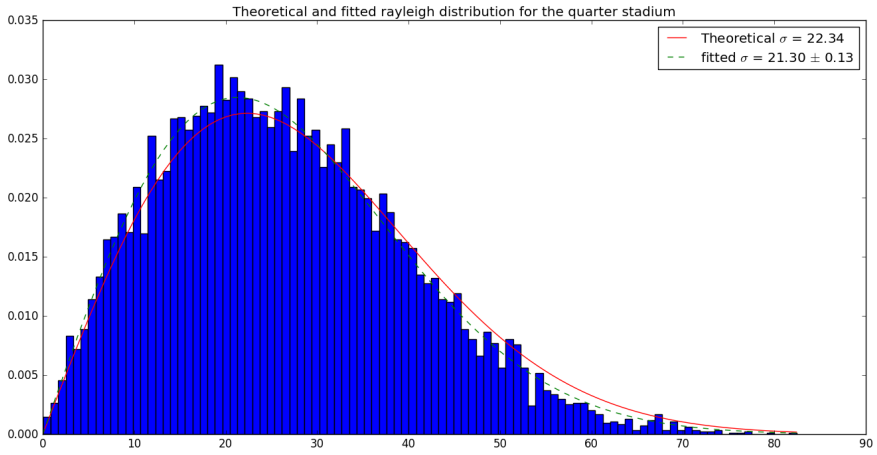

Figure 13: Histogram of the intensity of the pixels from a simulation in a quarter stadium with 1000 reflections. This is Rayleigh distributed with a similar parameter σ as theoretically expected.

The intensity distribution in this case is in agreement with our theoretically calculated distribution. Our test would now say that this cavity is ergodic.

5.3 Rayleigh distribution due to chaos

We have seen that ergodic cavities follow the Rayleigh distribution with a σ of around $\sqrt{\frac{n}{2}}$. Another question worth asking is how m any reflections are needed for this behavior to emerge. One might expect that a field calculated using 5 or less reflections has a lot more structure than a random field. We will study the onset of chaos in a wave field by comparing the intensity histogram as we increase the amount of reflections inside an ergodic system.
In figure 14 we looked at the field and intensity histogram for low numbers of reflection.

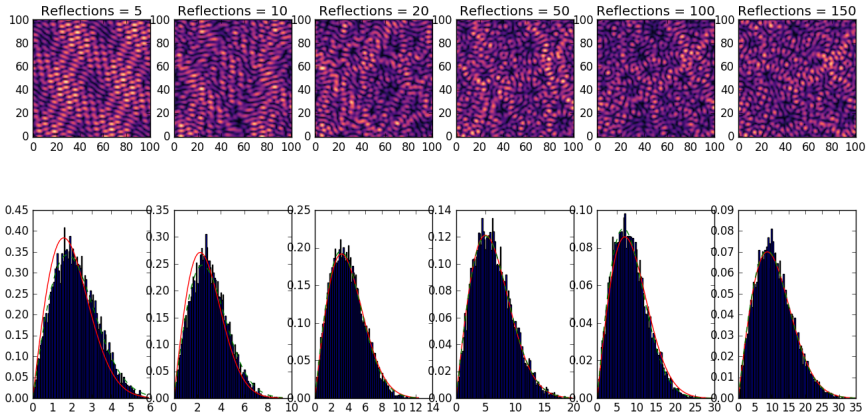

Figure 14: A comparison for low number of random reflection fields and how good the estimation is. There seems to be a slightly lower σ for n=5 and n=10.

Looking at the evolution of the field in figure 14 it seems that for the lowest numbers of n there still is some structure to the field. This structure correlates with a lower fitted σ compared to the theoretical σ. With this we will conclude that a differently valued and in most cases lower σ determines that a field is not (yet) fully chaotic. It is beyond the scope of this thesis but it might be interesting to look how well of a measure this is for the general structure of a field.

We can furthermore see in figure 14 that around 50 reflections the fitted Rayleigh distribution follows the expected Rayleigh distribution. Now with 100 reflections we can say for certain that the field converged to the theoretically expected distribution.

6 Convergence of the simulation

To check whether our model works correctly, we need to investigate its convergence behavior for many iterations. For us this means that we require that the used properties converge after a given number of reflections. This cutoff number additionally helps us to set a lower limit of necessary iterations to allow us to get physically correct information.

6.1 Convergence of the field

The first kind of convergence we look at is the convergence of the field. This means that every pixel in the field converges to a certain value, such that the picture of the field amplitude stays constant.
To test if this is true we simulated a closed cavity with no exits for $3.5 \cdot 10^5$ iterations. This simulation resulted in the conclusion that the field does not converge this way as can be seen in figure [15]. It is interesting that the field seems to be continuously changing with the amount of rays. In contrast, if we would apply losses to this simulation such that at every reflection only a percentage of the light will be reflected, we will get a converging field. This is because every pixel will be calculated as a geometric sum, which is known to be convergent.

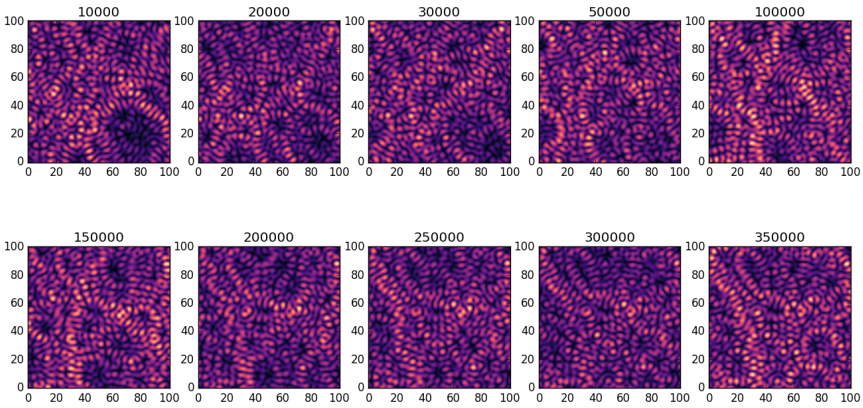

Figure 15: A simulation of the convergence of the field inside a closed of cavity. It can be seen that the field does not converge and seems to be continuously changing.

6.2 Number of reflections needed for convergence

It is helpful to know how many reflections the simulation of our quarter stadium cavity needs to get a reasonable converged result. Note that we can not use the distribution of the pixels as a measure for chaos because a clearly non chaotic pattern also can be approximated with a Rayleigh distribution in the same way as a chaotic field.
We will look at the number of reflections needed for a completely random field to obey our expected Rayleigh distribution.
For this we will compare the n dependency of our fit parameter σ from our Rayleigh distribution. This closely resembles the experiment we did earlier in chapter 4 with the expected value and standard deviation because the expected value is linearly dependent of σ. The result for a completely random field can be seen in figure 16

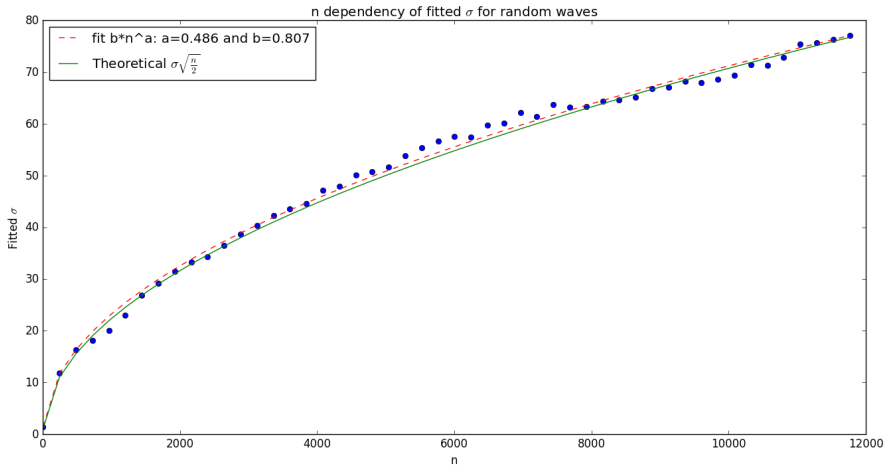

Figure 16: n dependency of fitted σ from a random wave field. This is in accordance with the theoretical σ.

We can see that the random waves have a fitted σ in accordance with the theoretical σ. We will now also test this for the quarter stadium cavity. The results for this can be seen in figure 17.

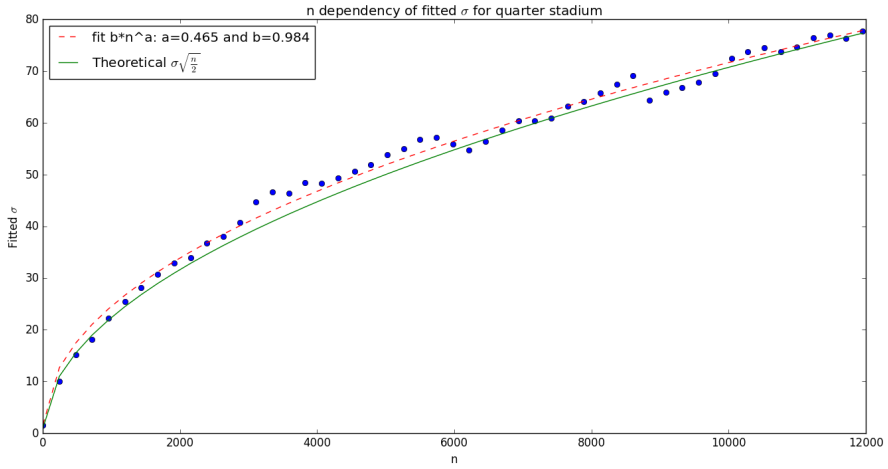

Figure 17: n dependency of fitted σ from a random wave from a quarter stadium. This is in accordance with the theoretical σ.

The results from the quarter stadium are also in accordance with the theoretical Rayleigh distribution. However, an aperiodic oscillation is visible in this data. For the explanation for this aperiodic oscillation we will look at an outlier simulation of the quarter stadium. The evolution of the fitted sigma can be seen in figure 18.

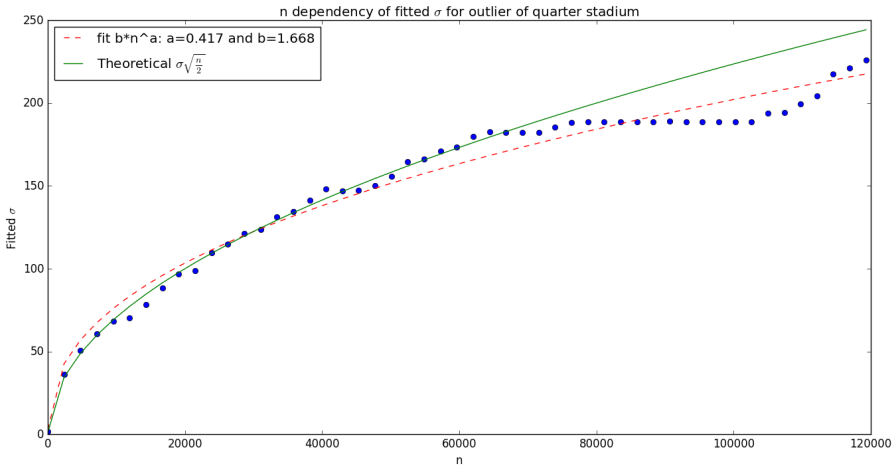

Figure 18: n dependency of fitted σ from a random wave from a quarter stadium. This simulation was a outlier which is not in accordance with the theoretical σ.

Up to 7000 reflections the datapoints in figure 18 follow the theoretical line well. After this point the datapoints seem to stay the same value and flat line. For this situation figure 19 gives more insight by showing the angle at which the wave propagates for every reflection. The flat lining of the fitted Rayleigh parameter coincides with an ordered mode of reflecting in the cavity.

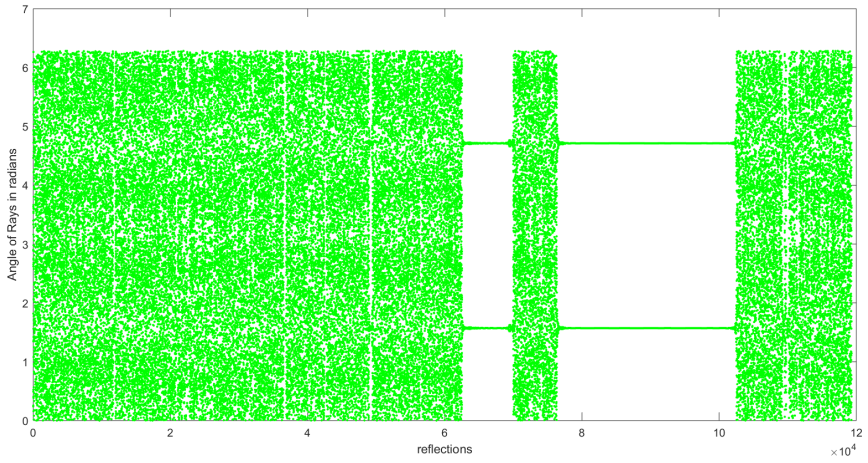

Figure 19: Angle of propagation for different reflections for the outlier of the quarter stadium. There is a large part of ordered reflections.

This ordered mode of reflection is due to the ray reflecting up and down in the right side of the cavity which is practically a square box. This ordered mode has no influence on the distribution of the intensity of the field due to mostly destructive interference. This results in the field staying constant during this ordered mode of reflections.

This explains the downwards motion of the aperiodic oscillation. The upwards motion can be explained intuitively. After an ordered regime we continue in the chaotic regime for a longer time.

Now for increasing time we get a larger percentage of the bounces from a chaotic regime with less destructive interference and behavior closer to random waves with a know n dependency of $\sqrt{n}$. This means we get an upward motion. Repeating this randomly might show something that looks like a wave-like structure.

This behavior is a result of how this model is constructed. Implementing losses might solve this problem and might be interesting for further research.

7 Outlook

In the course of this thesis, several interesting aspects arose that are beyond the scope of the thesis. Specifically related to introducing loss-channels in the cavity. These starting points for future investigations might lead to further understanding of the occurrence of certain features in the field of the cavity, as well as bringing the numerically calculated results in even closer agreement with experimental studies.

Most importantly, the experimental cavity exhibits scattering losses, meaning light can escape, which is not implemented in the model discussed. Loss can be implemented in ray tracing in 2 ways. The first is by assuming the ray to have completely exited the cavity when the loss occurs. If this loss occurs we continue the simulation with a new ray entering from the entrance. The second implementation of loss can be done by multiplying the amplitude of the simulated wave by a factor smaller than one every time a loss occurs. It might be interesting to compare both methods.
Implementing losses would make the simulated field convergent as stated in chapter 6.1. If the convergence of the simulated spatial field distribution is desired I would suggest implementing the second variant of losses.

7.1 General losses inside the cavity

In general there are 2 kind of losses in the physical cavity. One kind of loss is waves being (partially) transmitted instead of perfectly reflected on the cavity boundary. The second kind of loss is waves dissipating from the cavity into the z direction. This loss has a chance of occurring any time, assuming there are imperfections in the silicon slab from which the wave can scatter. This loss is dependent on the distance traveled of a single ray. So one might try implementing loss depending on this traveled distance.
It is not yet clear which of these losses, if any, dominate. It might be interesting to research the dominating loss and implement this in the ray tracing model.

7.2 Modelling exit in quarter stadium

A interesting part of the physical experiment are the exiting wave guides. Working on this thesis introducing an exit in the simulation of the quarter stadium cavity has been started. This exit is in the upper right corner of the cavity. This exit exists as a wave guide in the experimental cavity and can be seen in figure 1.

However, as a first step here we assumed the light to always completely exit trough the wave guide, meaning we continue the simulation with a new ray at the entrance of the cavity until the number of reflections of interest has been reached. An example of a simulated trajectory with these assumptions can be seen in figure 20. It can be seen that the density of rays is not homogeneous anymore, which might result in a deviation form a perfectly chaotic behavior and some kind of gap in phase space.

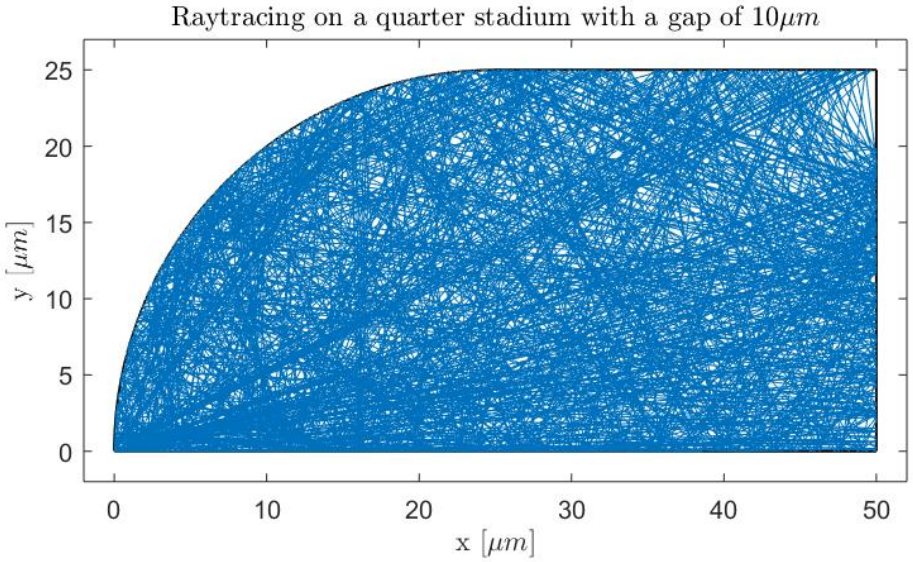

Figure 20: Simulation of ray tracing in a quarter billiard stadium with a gap of $10\mu m$ in the upper right corner.

The size of this gap changes the field behavior. Simulation of the field resulting from different gap sizes can be seen in figure 21. For the simulations with a gap size below $20\mu m$ we find a field comparable to a completely random simulated field as in figure 4. For larger gap sizes we slowly see a directional structure in the field. It seems more right traveling waves are present. This is due to light escaping our cavity trough the gap and not reflecting back into the cavity. Note that we can not deduce from this plot the overall propagation direction of the light. However, we can reason the waves are traveling to the right, because every ray starts in the bottom left corner and can escape on the right side. This should resulting in an abundance of right traveling waves.

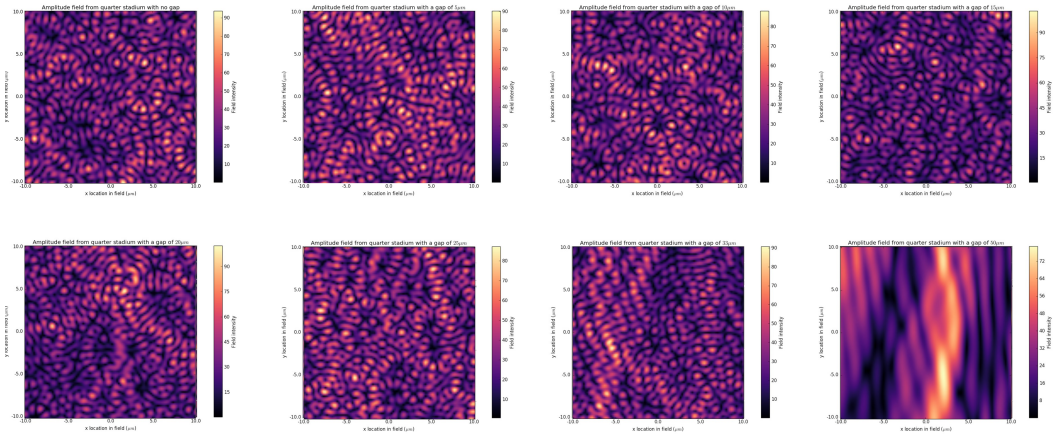

Figure 21: Simulations of a field in a quarter billiard stadium with different sized gaps between $0\mu m$ and $50\mu m$ in the upper right corner.

Investigation around the impact of introducing this gap might be interesting for further research as it was beyond the scope of this thesis. Different and more realistic assumption are possible for the interaction of light with the exiting wave guide. The implementation of this wave guide can be done by assuming a loss due to this wave guide. This loss can be modelled using a probability of reflection or a fraction reflecting as stated. For further research we recommend modeling an angle dependent probability or fraction based on the acceptance angle of the exiting wave guide.

8 Conclusion

In this thesis we have looked at different aspects of chaos in an ergodic cavity.

In a fist step, we showed that the quarter stadium cavity is chaotic because it has a positive Lyapunov exponent by simulating multiple trajectories, resulting in a positive Lyapunov exponent for all of them. This does not immediately mean it is also ergodic but strongly suggests it. Furthermore, the Lyapunov exponent for trajectories in a circular billiard has been investigated. We proved that all trajectories have a Lyapunov exponent of 0 meaning nearby trajectories do not diverge.

We additionally showed that the intensity of completely random waves is Rayleigh distributed with the theoretical parameter of $\sigma = \sqrt{\frac{n}{2}}$. Fields with more order than completely random fields also seem to follow this Rayleigh distribution, which suggests that this distribution is more generally a property of wave fields. However, more ordered fields seem to have a different distribution parameter compared to completely random fields. Determining this distribution parameter might be a good test for determining how ordered an intensity field is.

Our simulation has a $\sigma < \sqrt{\frac{n}{2}}$ while we expected it to be equal to $\sqrt{\frac{n}{2}}$. We conclude that this diverging from randomness is due to a highly structured way of reflecting in parts of the cavity which destructively interferes with itself, lowering the distribution parameter.

The field intensity distribution being Rayleigh distributed with the right parameter might be a good test for how ordered a wave field is in further research around this chaotic cavity and can help a lot with analyzing the implementation of losses in the quarter stadium cavity.

I also would like to thank Johan Dubbeldam, Kobus Kuipers, Thomas Bauer and Thijs van Gogh for helping me with writing this thesis during a difficult time for everyone.

References

[1] P. Cvitanovi et al. *Chaos Classical and Quantum*. Copenhagen: Niels Bohr Inst., 2016. URL: http://ChaosBook.org/.

[2] John D. Joannopoulos et al. *Photonic Crystals: Molding the Flow of Light (Second Edition)*. 2nd ed. Princeton University Press, 2008. ISBN: 0691124566.

[3] C. Liu et al. "Triggering extreme events at the nanoscale in photonic seas". In: *Nature Physics* 11 (Mar. 2015), p. 358. URL: https://doi.org/10.1038/nphys3263.

[4] Daniel McFadden. *STATISTICAL TOOLS*. Massachusetts, 2000.

[5] R. Markarian N. Chernov. *Introduction to the Ergodic Theory of Chaotic Billiards*. 2001.

[6] John A. Rice. *Mathematical Statistics and Data Analysis*. 3rd ed. Brooks/Cole, Cengage Learning, 2007.